On Companding Schemes for PAPR Reduction in OFDM Systems Employing Higher Order QAM

Sana Mazahir and Shahzad Amin Sheikh

***Abstract*—Large peak-to-average power ratio (PAPR) of the signal is an imperative problem in orthogonal frequency division multiplexing (OFDM) systems, as it impedes the efficient design of their analog front end. Companding is a well-known technique that reduces the PAPR by using a deterministic amplitude transform, which is designed by assuming Rayleigh distribution for the signal amplitude. But in OFDM systems employing higher order QAM, like 16- or 64-QAM, this probabilistic model is insufficient to model the true characteristics of the signal. This is due to the stochastic nature of average symbol power, which alters the complete amplitude distribution from one OFDM symbol to another. This leads to degradation in the companders' PAPR reduction performance. In this paper, we propose two novel schemes that modify the companding operation to accommodate the randomness of symbol power. Probabilistic analysis of symbol's average power, in relationship with the amplitude of its constituent samples, is carried out. This yields the theoretical framework employed in the design of the proposed low-complexity solutions. The proposed schemes essentially make the companding operation itself nondeterministic/adaptive, i.e., it adjusts to comply with the changing symbol amplitude distribution during application runtime.**

***Index Terms*—Orthogonal frequency division multiplexing (OFDM), peak-to-average power ratio (PAPR), companding transform, QAM.**

I. Introduction

ORTHOGONAL frequency division multiplexing (OFDM) has been extensively deployed in high speed wireless communications, including broadband internet access systems and digital audio/video broadcasting. It offers the advantages of high spectral efficiency and immunity to multipath fading [1]. However, being a multi-carrier modulation technique, OFDM signal has a highly fluctuating, noise-like envelope. This increases the dynamic range of the signal, due to which it experiences non-linear distortion introduced by the high-power amplifier (HPA) at the transmitter's front-end. Consequently, bit error rate (BER) and out-of-band interference (OBI) levels are elevated.

Peak-to-average power ratio (PAPR) is typically used to quantify the dynamic range of OFDM signals. Several PAPR reduction techniques have been proposed, which can be classified into three types: signal distortion techniques, multiple signaling/probabilistic schemes and coding techniques [2], [3]. Among the signal distortion techniques, companding transforms are gaining a lot of interest due to their low implementation complexity and capability of efficiently trading between PAPR and BER.

Several companding transforms have been presented [4]–[18]. In all these designs, *OFDM signal amplitude is modeled using the Rayleigh distribution with a constant average power parameter*. The transforms are derived with the objective of modifying this distribution, subject to various constraints. The compander design has been considered to be independent of symbol period and constellation type [4]. However, we found that a compander's performance is affected by these parameters (see Section III). In all the above-mentioned researches, complete performance evaluation (PAPR, BER and OBI) has been presented only for 4-QAM/QPSK based OFDM signals. We found that the PAPR reduction performance degrades in case of higher order QAM, like 16 and 64-QAM.

The reason for the degradation in the companders' performance can be explained by noting that with 4-QAM/QPSK, the average power of all OFDM symbols remains constant. In contrast, when higher order QAM constellations are used, average symbol power is a *random variable*. *Since the Rayleigh distribution is specified by a constant average power parameter, the stochastic nature of average symbol power renders it insufficient to approximate the true amplitude distribution within an OFDM symbol duration*. In conventional companding, all the symbols are transformed using the same deterministic function, which is designed by assuming a fixed Rayleigh distribution for signal amplitude, irrespective of the constellation type. Hence, the prevalent randomness in average power of an OFDM symbol and its relationship with the amplitude distribution of the constituent samples is neglected in these schemes. Consequently, they do not perform optimally with higher order QAM. It should be noted here, that the fixed Rayleigh distribution effectively models the long-term signal amplitude statistics, i.e., when a large number of OFDM symbols are collectively considered. However, PAPR is always evaluated per OFDM symbol [2]. Hence, for the design optimization of companding schemes, it is logical to consider the signal's amplitude distribution correspondingly.

In this paper, we present *two novel schemes, namely adjustable-parameter companding (APC) and adaptive constellation scaling (ACS). The main idea is to enable the*

Manuscript received October 12, 2015; revised December 11, 2015; accepted December 16, 2015. Date of publication January 12, 2016; date of current version August 31, 2016.

The authors are with the Department of Electrical Engineering, College of Electrical and Mechanical Engineering, National University of Sciences and Technology, Rawalpindi 46000, Pakistan (e-mail: sana75@ee.ceme.edu.pk; sheikh.shahzadamin@gmail.com).

Color versions of one or more of the figures in this paper are available online at http://ieeexplore.ieee.org.

Digital Object Identifier 10.1109/TBC.2015.2511627

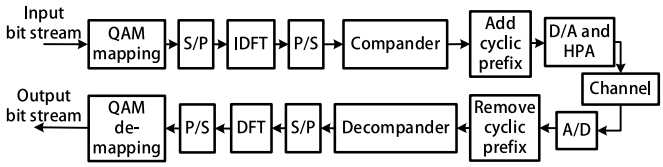

Fig. 1. OFDM system model with conventional companding.

compander to comply with the changing amplitude distribution from one OFDM symbol to another. In order to understand and assess the problem, we first conduct some case studies in Section III, in which we evaluate companding transforms with respect to changing OFDM specifications. Motivated by the observations thereof, *we develop the analytical probabilistic model of average symbol power and its relationship with the amplitude distribution* in Section IV. The derived probability distributions are then utilized in the design of the proposed schemes, in such a way that the randomness of average symbol power is accommodated in the companding operation. The proposed solutions are presented in Section V. Simulations are carried out to demonstrate that the proposed schemes outperform the conventional ones with regard to PAPR, BER and OBI. Detailed performance evaluation is presented in Section VI. The proposed schemes have been effectively applied to enhance the performance of three state-of-the-art companders. It is demonstrated that *the proposed schemes are capable of jointly reducing the PAPR and BER, while keeping OBI level unaffected*, which is not possible in conventional signal distortion techniques.

II. OFDM System Model

Fig. 1 shows a typical OFDM system model with a companding scheme. The oversampled, discrete time, complex envelope of the transmitted OFDM signal is given as follows:

$$x_n = \frac{1}{\sqrt{NL}} \sum_{k=0}^{NL-1} X_k \exp\left(\frac{j2\pi kn}{NL}\right), \text{ for } 0 \le n \le NL-1 \quad (1)$$

where X_k comes from the input symbol vector $[X_0, X_1, X_2, \ldots, X_{\frac{N}{2}-1}, \underbrace{0, \ldots, 0}_{N(L-1)}, X_{\frac{N}{2}}, \ldots, X_{N-1}]$. N is the number of sub-carriers including N_d data carriers, N_p pilot carriers and null carriers (for guard band and DC). L is the oversampling factor. Data symbols are modulated using a given QAM constellation.

Since all the data symbols are independently and randomly sampled from QAM constellation, each sample x_n is a random variable generated by the weighted average of independent and identically distributed (IID) random variables. When N is large, x_n can be approximated as a complex Gaussian random process by the central limit theorem (CLT) approximation. Hence, the signal amplitude $|x_n|$ is a Rayleigh random process. Its probability density function (PDF) is given as follows:

$$f_A(x) = \frac{2x}{\sigma_x^2} \exp\left(-\frac{x^2}{\sigma_x^2}\right) \quad (2)$$

where A is the random variable associated with $|x_n|$, for $0 \le n \le NL-1$, and $\sigma_x^2 = E[|x_n|^2]$ is the average signal power.

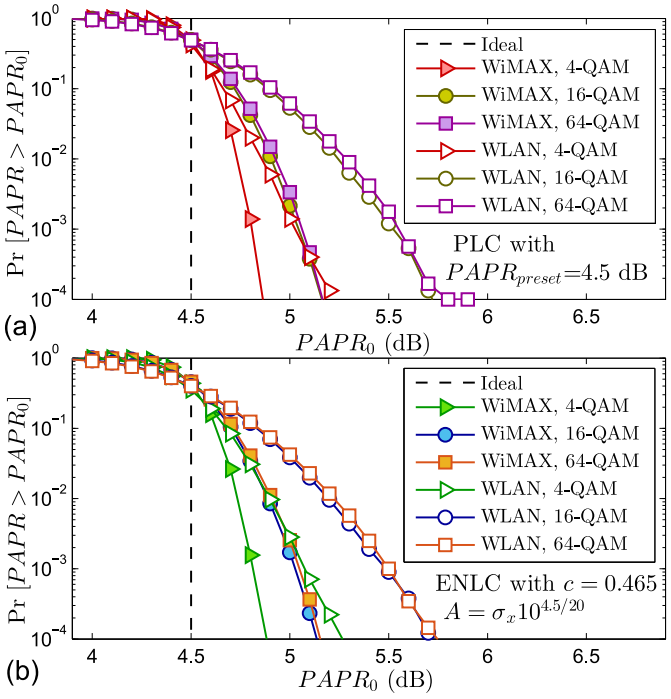

Fig. 2. CCDFs of PAPR for (a) PLC, and (b) ENLC for various standards.

PAPR of an OFDM symbol is defined as the ratio of peak power to average power *within a symbol duration* [2], i.e.,

$$\text{PAPR (dB)} = 10\log_{10}\left(\frac{\max\limits_{0\le n\le NL-1}|x_n|^2}{\frac{1}{NL}\sum\limits_{n=0}^{NL-1}|x_n|^2}\right) \quad (3)$$

PAPR is evaluated using empirical complementary cumulative distribution functions (CCDFs) of PAPR,

$$CCDF_{PAPR}(PAPR_0) = \Pr[PAPR > PAPR_0] \quad (4)$$

A. Companding for PAPR Reduction

The compander in Fig. 1 is an amplitude transform $T(.)$, i.e., its output signal is $y_n = T(|x_n|)\text{sgn}(x_n)$. The transform $T(.)$ compresses the larger amplitudes to reduce the peak power and amplifies smaller amplitudes to increase SNR [4]. PAPR is reduced at the expense of non-linear distortion. The key challenge in the design of a companding scheme is to minimize the effects of this distortion while realizing the desired PAPR.

III. Motivational Study

Fig. 2 shows PAPR reduction performance evaluation for the piecewise linear compander (PLC) [6] and the efficient non-linear compander (ENLC) [11] for various OFDM specifications, given in Table I. *Wireless local area network* (WLAN), based on IEEE 802.11a and *fixed worldwide interoperability for microwave access* (WiMAX), based on IEEE 802.16d, are used to simulate the effect of changing number of sub-carriers.

TABLE I
SPECIFICATIONS OF WLAN AND FIXED WIMAX

Standard	N	N_d	N_p	Modulation
WLAN	64	48	4	4-QAM, 16-QAM, 64-QAM
Fixed WiMAX	256	192	8	4-QAM, 16-QAM, 64-QAM

A. Effect of Constellation Type

1) Observations: Fig. 2 shows that, as compared to 4-QAM, variance of PAPR around the ideal value increases in case of 16 and 64-QAM. For fewer sub-carriers, i.e., in WLAN, the degradation is greater than that for larger number of sub-carriers, i.e., in WiMAX. With PLC, PAPR at CCDF= 10^{-3} increases by 0.5 dB in WLAN whereas in WiMAX, it increases by 0.25 dB, when 4-QAM is replaced with 16-QAM. Similar trends are observed with ENLC.

2) Discussion: These observations can be explained by noting that all these transforms are designed by assuming Rayleigh PDF, given in Eq. (2), for signal amplitude. In an OFDM signal constructed using 16 or 64-QAM, the average power is not equal to σ_x^2 for all symbols; rather it is a random variable (see Section IV for detail). Consequently, the amplitude distribution within an OFDM symbol duration exhibits deviation from the long-term average, which is more pronounced in case of fewer data carriers per symbol. This is a manifestation of the *law of large numbers* (LLN), which predicts that the average symbol power will be closer to its expected value if the number of superimposed carriers is larger. When sub-carriers per symbol are too few to constitute a large enough data set, the variance of average symbol power increases. This eventually leads to larger deviation of PAPR of the compander's output from its desired/ideal value.

B. Applications

Several prevailing and emerging wireless communication standards specify 16-QAM and 64-QAM as modulation schemes in OFDM systems for high data rate support. Hence, we shall be using these two constellations throughout this article. Standards include IEEE 802.11a/g for WLAN [19], IEEE 802.16 for fixed and mobile WiMAX [20], the European ETSI HIPERLAN/2 [19], *long term evolution* (LTE) [21] and *digital video broadcasting terrestrial* (DVB-T) [22].

WLAN and HIPERLAN/2 have similar OFDM parameters [19]. WiMAX and LTE specifications accommodate number of sub-carriers ranging from 128 to 2048 to cover a wide range of bandwidths [20], [21]. Moreover, the increase in BER due to companding is also larger with 16-QAM than that with 4-QAM [5], [6], [11], [13]. Thus, with conventional companding, there are several practical applications in which we expect significant degradation in the overall performance of the system due to the above-discussed problem. Therefore, in this paper, we develop solutions to mitigate this degradation.

IV. STOCHASTIC MODELING OF AVERAGE POWER AND AMPLITUDE OF OFDM SYMBOLS

In this section, probability distribution of the average power of OFDM symbols is derived and its relationship with the amplitude distribution is modeled. This yields the theoretical framework used to develop the schemes in Section V.

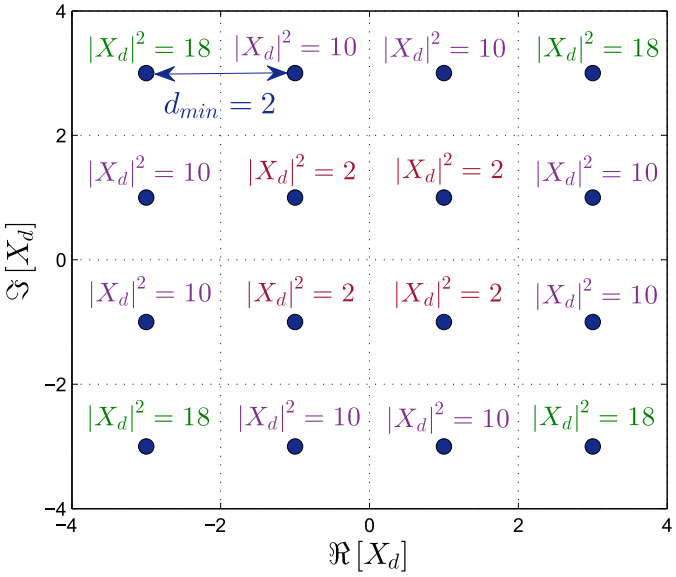

Fig. 3. Symbol-to-energy mapping for 16-QAM constellation.

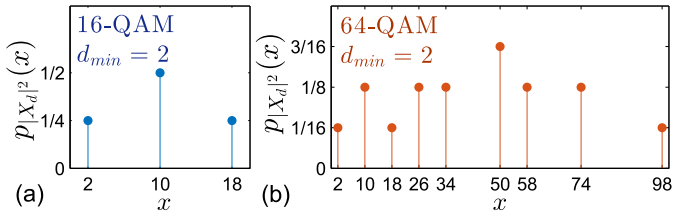

Fig. 4. PMFs of $|X_d|^2$ for (a) 16-QAM and, (b) 64-QAM constellations.

A. Distribution of OFDM Symbol Average Power

Let S represent the random variable associated with the average power of an OFDM symbol. Using the Parseval's theorem of discrete Fourier transform (DFT), we can write

$$S = \frac{1}{NL}\sum_{n=0}^{NL-1}|x_n|^2 = \frac{1}{NL}\sum_{k=0}^{NL-1}|X_k|^2 \tag{5}$$

Average energy of M-ary square QAM is given by $\sigma^2_{SQAM} = d^2_{min}(M-1)/6$, where d_{min} is the distance between nearest neighbors in the constellation. If σ_p^2 is the average energy of pilot symbols, then σ_x^2 in Eq. (2) is given as:

$$\sigma_x^2 = E[S] = \frac{1}{NL}\left(N_d\sigma^2_{SQAM} + N_p\sigma_p^2\right) \tag{6}$$

Let $D = \{d_1, d_2, ..., d_{N_d}\}$ and $P = \{p_1, p_2, ..., p_{N_p}\}$ be the sets containing indexes of data carriers and pilot carriers, respectively. Then $X_{d_1}, X_{d_2}, ..., X_{d_{N_d}}$ are IID random variables sampled from a QAM constellation. Let X_d represent any one of these random variables. In case of 16 and 64-QAM, $|X_d|^2$ is also a random variable, because the symbol vectors in the constellation have different amplitudes. This is in contrast with 4-QAM in which $|X_d|^2$ is a constant. Symbol-to-energy mapping for 16-QAM constellation is shown in Fig. 3. Assuming that all QAM symbols are equally likely, probability mass

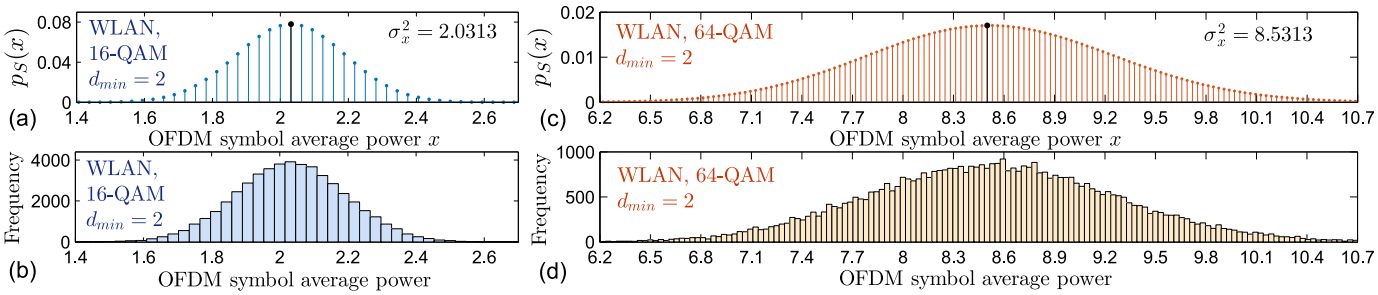

Fig. 5. Comparison of theoretical and empirical OFDM symbol average power distributions. (a) $p_S(x)$ with 16-QAM, (b) Histogram of symbol power with 16-QAM, (c) $p_S(x)$ with 64-QAM and, (d) Histogram of symbol power with 64-QAM.

functions (PMFs) of $|X_d|^2$ for 16-QAM and 64-QAM are evaluated and shown in Fig. 4.

Now, S, given in Eq. (5), can be re-written as follows:

$$S = \underbrace{\frac{1}{NL}\sum_{k\in D}|X_k|^2}_{\text{random}} + \underbrace{\frac{1}{NL}\sum_{k\in P}|X_k|^2}_{\text{constant}} + \underbrace{\frac{1}{NL}\sum_{k\in (P\cup D)'}|X_k|^2}_{=0,\text{ (guard band and DC)}}$$
$$= \frac{1}{NL}\left(\left|X_{d_1}\right|^2 + \left|X_{d_2}\right|^2 + \ldots + \left|X_{d_{N_d}}\right|^2\right) + \frac{N_p}{NL}\sigma_p^2 \quad (7)$$

Let $S_d = NLS - N_p\sigma_p^2$, so that

$$S_d = \left|X_{d_1}\right|^2 + \left|X_{d_2}\right|^2 + \ldots + \left|X_{d_{N_d}}\right|^2 \quad (8)$$

Each of $|X_{d_1}|^2, |X_{d_2}|^2, \ldots, |X_{d_{N_d}}|^2$ is distributed according to PMF $p_{|X_d|^2}(x)$. Since *the PMF of sum of independent random variables is equal to the convolution of PMFs of individual random variables* [23], so S_d has the following distribution:

$$p_{S_d}(x) = \underbrace{p_{|X_{d_1}|^2}(x) * p_{|X_{d_2}|^2}(x) * \ldots * p_{\left|X_{d_{N_d}}\right|^2}(x)}_{N_d-1 \text{ convolutions}} \quad (9)$$

where $p_{|X_{d_1}|^2}(x) = p_{|X_{d_2}|^2}(x) = \ldots = p_{|X_{d_{N_d}}|^2}(x) = p_{|X_d|^2}(x)$. Now the PMF $p_S(x)$ is found as follows:

$$p_S(x) = \Pr[S = x] = \Pr\left[\frac{S_d + N_p\sigma_p^2}{NL} = x\right] \quad (10)$$

$$p_S(x) = p_{S_d}\left(NLx - N_p\sigma_p^2\right) \quad (11)$$

The derived PMFs and histograms of S, obtained by evaluating S for 50000 simulated OFDM symbols, are compared in Fig. 5. The non-zero variance of symbol power around the mean σ_x^2 can be clearly observed. It is the effect of this variance that is manifested in the degradation in the PAPR reduction performance observed in Section III.

Interestingly, we found that, although $\mathrm{Var}(S)$ is larger with 64-QAM ($\mathrm{Var}(S) = 0.5332$) than that in 16-QAM ($\mathrm{Var}(S) = 0.0254$), but the relative standard deviations, i.e., $\sqrt{\mathrm{Var}(S)}/\sigma_x^2$, in both cases are very close (0.078 in 16-QAM, 0.085 in 64-QAM). PAPR also represents peak power relative to average power. Hence, the deviation of PAPR from the ideal value is almost identical for both constellations (see Fig. 2).

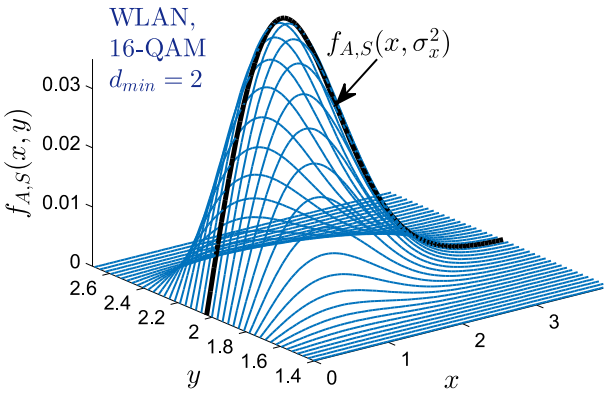

Fig. 6. Joint symbol average power and amplitude distribution.

B. Amplitude Distribution Within an OFDM Symbol

Since S deviates from σ_x^2, Rayleigh PDF in Eq. (2) is insufficient to model the amplitude distributions within individual OFDM symbols. Rather, they can be more appropriately characterized by a *family of conditional Rayleigh distributions*. The parameter of a Rayleigh distribution, belonging to the said family, can have any value for which $p_S(.) \neq 0$. *The probability that the amplitude distribution of a randomly generated OFDM symbol conforms to Rayleigh distribution with parameter y is equal to $p_S(y)$.*

The PDF of amplitude of a sample $|x_n|$ (represented by A) belonging to an OFDM symbol with $S = y$, is found by modifying the PDF in Eq. (2) as follows:

$$f_A(x \mid S = y) = \frac{2x}{y}\exp\left(-\frac{x^2}{y}\right) \quad (12)$$

The distributions in Eq. (12) were validated by comparing them with distributions estimated from simulated data. The joint PDF of amplitude and symbol power is given as follows:

$$f_{A,S}(x, y) = \frac{2x}{y}\exp\left(-\frac{x^2}{y}\right)p_S(y) \quad (13)$$

The joint distribution is shown in Fig. 6. For every possible value of S, there is a corresponding Rayleigh PDF for A. Hence, the random variable A *is dependent on* S.

A companding transform is designed to modify the amplitude distribution. Consequently, it will also yield closer-to-desired output if it recognizes and deals with this dependence

of amplitude on symbol's average power. To accomplish this objective, we present two novel schemes in the next section.

V. Proposed Solutions

In Sections III and IV, we established that since the amplitude distribution within an OFDM symbol duration depends on the average power S of that symbol, the companding operation should also adapt to S. This is the foundational idea for both the schemes presented in Sections V-B and V-C. In order to cut down the overhead on complexity and throughput involved in these schemes, we first classify the OFDM symbols on the basis of S in Section V-A.

A. Classification of OFDM Symbols

1) Motivation: Theoretically, S can attain values over a large range. For instance, in case of WLAN with 16-QAM, S can attain 105 values, ranging from 0.4063 to 3.6563. However, the probability of S having these values is of the order of 10^{-32}. $p_S(x)$ for this case is shown in Fig. 5(a) (complete range of S is not shown). Similarly in WLAN with 64-QAM, S can have 621 different values, with probabilities as small as 10^{-63}. This implies that it would be inefficient to force the companding operation to adjust differently for every single value of S. Instead, the computational and bandwidth resources would be more cost-effectively utilized if the process governing the adaptivity to S is designed by assigning appropriate weightages to average and outliers.

In Section III-A, we discussed that the variance of PAPR around its ideal value is due to the variance of S. Therefore, if the variance of S is reduced, the output PAPR will also come closer to ideal. Hence, *in order to cut down the overhead, we propose to classify OFDM symbols into J groups, each with smaller than total variance of S and to design only J adaptations of the compander.*

2) Criteria for Classification: Consider the ensemble of OFDM symbols constructed from a higher order QAM constellation with given N, N_d and N_p. The ensemble can be divided into J subsets, such that within each subset, the variance of S of the constituent symbols is smaller as compared to that in the complete ensemble. Let $[s_0, s_1], (s_1, s_2], ..., (s_{J-1}, s_J]$ be J consecutive and disjoint intervals of the symbol power S, where $s_0 < s_1 < s_2 < \ldots < s_J$. $s_0 = \min(S)$, $s_J = \max(S)$ and $s_1, s_2, ..., s_{J-1}$ are such that the variance within each interval is equal, i.e.,

$$\begin{aligned}\mathrm{Var}[S \mid S \in [s_0, s_1]] &= \mathrm{Var}[S \mid S \in (s_1, s_2]] = \ldots \\ &= \mathrm{Var}\big[S \mid S \in (s_{J-1}, s_J]\big] \end{aligned} \tag{14}$$

For $J \geq 2$, S in each interval varies over a smaller range than $\max(S) - \min(S)$. We found that using the criteria in Eq. (14), variance of S within each interval comes out to be smaller than the total variance, i.e., $\mathrm{Var}\big[S \mid S \in [s_{j-1}, s_j]\big] < \mathrm{Var}[S]$ for $j = 1, 2, ..., J$. If we design companding operation separately and independently for each subset, then the effect of variance of S on each adaptation of the compander will be smaller, which eventually leads to reduced variance of PAPR in every subset. The conditions in Eq. (14) suggest that the PAPR reduction performance will be approximately similar in all the J subsets, which means that overall variance of PAPR will also be reduced. The conditional variances in Eq. (14), for $j = 1, 2, ..., J$, are evaluated as follows:

$$\begin{aligned}\mathrm{Var}\big[S \mid S \in [s_{j-1}, s_j]\big] &= \mathrm{E}\left[\left(S - \sigma_{xj}^2\right)^2 \mid S \in [s_{j-1}, s_j]\right] \\ &= \sum_{x \in [s_{j-1}, s_j]} \left(x - \sigma_{xj}^2\right)^2 p_S\big(x \mid S \in [s_{j-1}, s_j]\big) \end{aligned} \tag{15}$$

where σ_{xj}^2 is the expected value of S within the subset j, i.e.,

$$\begin{aligned}\sigma_{xj}^2 &= \mathrm{E}\big[S \mid S \in [s_{j-1}, s_j]\big] \\ &= \sum_{x \in [s_{j-1}, s_j]} x\, p_S\big(x \mid S \in [s_{j-1}, s_j]\big) \end{aligned} \tag{16}$$

Hence, σ_{xj}^2 is the overall average power of the symbols belonging to the j^{th} subset. It should be noted here that the notation $[s_{j-1}, s_j]$ is interpreted as $(s_{j-1}, s_j]$ for $j \geq 2$. Using the definition of conditional probability, the conditional PMF, in Eqs. (15) and (16), is found as follows:

$$\begin{aligned} p_S\big(x \mid S \in [s_{j-1}, s_j]\big) &= \frac{\Pr\big[S = x, S \in [s_{j-1}, s_j]\big]}{\Pr\big[S \in [s_{j-1}, s_j]\big]} \\ &= \begin{cases} \dfrac{p_S(x)}{\sum_{x \in [s_{j-1}, s_j]} p_S(x)}, & \text{for } x \in [s_{j-1}, s_j] \\ 0, & \text{otherwise} \end{cases} \end{aligned} \tag{17}$$

Algorithm 1 is used to evaluate $s_0, s_1, ..., s_J$, when J is a power of 2. In this algorithm, we successively bisect the entire range of S. In each iteration, the interval with maximum variance of S is divided into two, such that the variances of S in the two new intervals are approximately equal.

Algorithm 1 Evaluation of $s_0, s_1, ..., s_J$

1: Input arrays $p_S(x)$ and x, such that $p_S(x) \neq 0$.
2: Input number of subsets J.
3: Set $s_0 = \min(x)$, $s_J = \max(x)$.
4: Initialize array $S_{arr} = [s_0, s_J]$.
5: Initialize variables $u = s_0$, $v = s_J$.
6: Find $w \in [u, v]$, such that it minimizes $|\mathrm{Var}(S \mid S \in [u, w]) - \mathrm{Var}(S \mid S \in [w, v])|$, where the conditional variances are evaluated using Eqs. (15), (16) and (17).
7: Append w to S_{arr} and sort S_{arr} in ascending order.
8: Find $k \in \{1, 2, 3, ..., \mathrm{length}(S_{arr}) - 1\}$, such that $\mathrm{Var}(S \mid S \in [s_k, s_{k+1}])$ is maximum.
9: Update $u = s_k$, $v = s_{k+1}$.
10: If $\mathrm{length}(S_{arr}) < J + 1$, repeat steps 6-9; Otherwise output $S_{arr} = [s_0, s_1, s_2, ..., s_J]$ and terminate.

3) Amplitude Distribution Within Subsets: The j^{th} subset of OFDM symbols, $\underline{\mathrm{x}}_{\mathbf{n}} = [x_0, x_1, ..., x_{NL-1}]$, is defined as:

$$\left\{\underline{\mathrm{x}}_{\mathbf{n}} \mid S\big(\underline{\mathrm{x}}_{\mathbf{n}}\big) \in \big[s_{j-1}, s_j\big]\right\} \tag{18}$$

where $S(\underline{\mathrm{x}}_{\mathbf{n}}) = (1/NL) \sum_{n=0}^{NL-1} |x_n|^2$, i.e., the average power of symbol $\underline{\mathrm{x}}_{\mathbf{n}}$. As discussed in Section IV, the amplitude distribution $f_A(.)$ of every sample belonging to an OFDM symbol is a function of the average power S of that symbol. Thus, by using the law of total probability [23] and

Eq. (12), the amplitude distribution of a sample belonging to any symbol $\underline{x}_{\mathbf{n}}$ in the j^{th} subset is given by the conditional PDF as follows:

$$\begin{aligned} f_A\big(x \mid S \in [s_{j-1}, s_j]\big) &= \sum_{y \in [s_{j-1}, s_j]} f_A(x \mid S = y) p_S\big(y \mid S \in [s_{j-1}, s_j]\big) \\ &= \sum_{y \in [s_{j-1}, s_j]} \frac{2x}{y} \exp\left(-\frac{x^2}{y}\right) p_S\big(y \mid S \in [s_{j-1}, s_j]\big) \end{aligned} \quad (19)$$

Eq. (19) is essentially the average of Rayleigh distributions with parameters in the range $[s_{j-1}, s_j]$. Alternatively, since the average power of all the samples in j^{th} subset is σ_{xj}^2, given in Eq. (16), and they are all Rayleigh distributed, so the conditional PDF in Eq. (19) can also be approximated as a Rayleigh PDF with parameter σ_{xj}^2, i.e.,

$$f_A\big(x \mid S \in [s_{j-1}, s_j]\big) \approx f_A\left(x \mid S = \sigma_{xj}^2\right) = \frac{2x}{\sigma_{xj}^2} \exp\left(-\frac{x^2}{\sigma_{xj}^2}\right) \quad (20)$$

In Fig. 7, the conditional cumulative distribution functions (CDFs), obtained as integrals of the PDFs in Eq. (20), are compared with the empirical CDFs, obtained from simulated OFDM signal. The empirical CDFs are evaluated by classifying the simulated symbols into J groups or subsets and the CDFs are estimated for each subset as given below:

$$\hat{F}_A\big(x \mid S \in [s_{j-1}, s_j]\big) = \frac{\text{Number of samples with } A \le x \text{ in } j^{th} \text{ subset}}{\text{Total number of samples in } j^{th} \text{ subset}} \quad (21)$$

It can be seen that the conditional distributions, obtained from Eq. (20), are in good agreement with those obtained from simulated data. It should be noted that both the PDF expressions above, given in Eqs. (19) and (20), were found to be in good agreement with the simulated distributions. For simplicity, we shall be using the PDFs in Eq. (20) in the development of schemes proposed in the next sub-sections.

In Fig. 7, we also observe *that $F_A(.)$ with different values of σ_{xj}^2 significantly differ from one another*. Therefore, a compander designed for one of them will not perform well for a symbol with another value of S. This is the mathematical reason for the degradation observed in Fig. 2 and is also the reason for designing many adaptations of the companding operation in the proposed schemes.

4) Mechanism for Selecting Companding Adaptation: The operation of companders with the schemes proposed in the next sub-sections is explained as follows:

- For each input OFDM symbol, S is calculated and a value of j is assigned by comparing S with $s_0, s_1, ..., s_J$.
- Then the signal is transformed by the companding adaptation that is designed for signal amplitude with Rayleigh distribution specified by parameter σ_{xj}^2.

The modified system with the two proposed schemes is illustrated in Fig. 8. Since DFT is a unitary transform, S can be evaluated from either frequency or time domain sequence, as given in Eq. (5). The number of non-zero elements in frequency domain sequence is smaller. Thus for low-complexity implementation, we have used the frequency domain sequence, which consists of complex QAM symbols. Complexity analysis is given in Section VI-E.

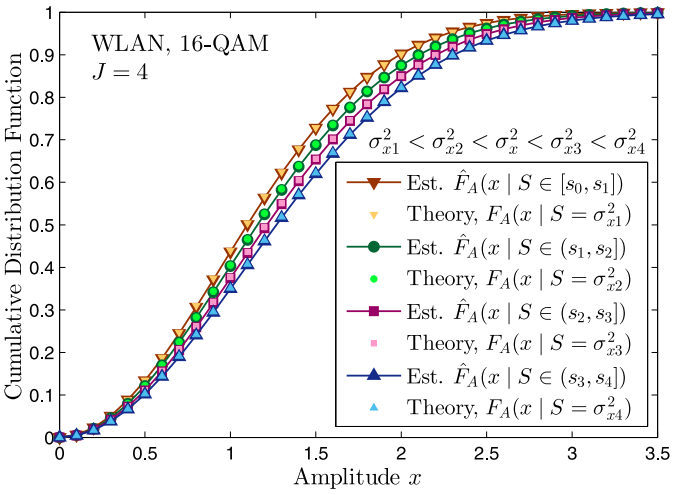

Fig. 7. Comparison of theoretical and simulated conditional distributions.

B. Adjustable-Parameter Companding (APC)

1) Main Idea: In this scheme, we *adjust the compander parameters according to the value of S of each input symbol*, as illustrated in Fig. 8.

2) Design of APC Parameters: The scheme essentially involves designing the compander parameters by assuming the signal amplitude to be Rayleigh distributed with parameter σ_{xj}^2, given in Eq. (16), if $S \in [s_{j-1}, s_j]$.

- The parameters for each $j = 1, 2, 3, ..., J$ can be independently calculated by substituting σ_x with σ_{xj} in the transform design equations and the compander can select from a parameter set during run-time.
- Alternatively, if the values of parameters at power σ_x^2 are known, then parameters for symbol with power σ_{xj}^2 can be evaluated as a function of these values and σ_x^2.

For instance, the piecewise linear compander (PLC) in [6] is specified by three parameters: clipping level A_c, inflexion point A_i and slope k, at average symbol power σ_x^2. The parameters for APC for a symbol belonging to j^{th} subset are found by substituting amplitude x with $(\sigma_{xj}/\sigma_x)x$ and σ_x with σ_{xj} in the design equations. The j^{th} triad of parameters comes out to be as follows:

$$\big(A_{cj}, A_{ij}, k_j\big)_{\text{PLC}} = \left(\frac{\sigma_{xj}}{\sigma_x} A_c, \frac{\sigma_{xj}}{\sigma_x} A_i, k\right)_{\text{PLC}} \quad (22)$$

Similarly, for the piecewise exponential compander (PEC) [5],

$$\big(A_{cj}, A_{ij}, \sigma_{xj}, d_j\big)_{\text{PEC}} = \left(\frac{\sigma_{xj}}{\sigma_x} A_c, \frac{\sigma_{xj}}{\sigma_x} A_i, \sigma_{xj}, d\right)_{\text{PEC}} \quad (23)$$

For the efficient non-linear compander (ENLC) [11],

$$\big(A_j, c_j, k_j, \sigma_{xj}\big)_{\text{ENLC}} = \left(\frac{\sigma_{xj}}{\sigma_x} A, c, \frac{\sigma_x^2}{\sigma_{xj}^2} k, \sigma_{xj}\right)_{\text{ENLC}} \quad (24)$$

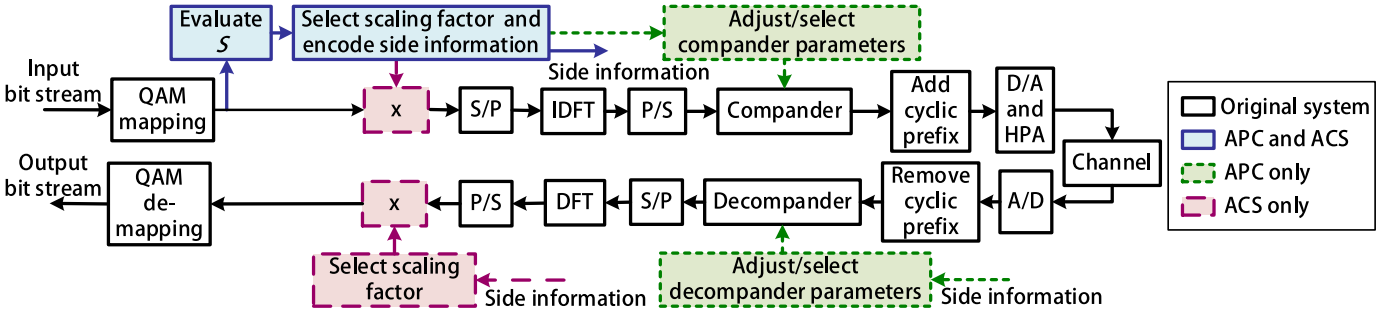

Fig. 8. Modified system with the proposed APC and ACS schemes.

3) Mathematical Definition of the APC Scheme: The APC scheme, using the PLC, is given as follows:

$$T_{\mathrm{APC}}(x) = T_{\mathrm{PLC}}\left(x; A_{cj}, A_{ij}, k_j\right), \quad \text{if } x \in \underline{\mathrm{x}}_{\mathbf{n}} \text{ and } S\left(\underline{\mathrm{x}}_{\mathbf{n}}\right) \in \left[s_{j-1}, s_j\right] \tag{25}$$

for $j = 1, 2, ..., J$. $T_{\mathrm{PLC}}(x; A_{cj}, A_{ij}, k_j)$ is the transform function for the PLC with parameters (A_{cj}, A_{ij}, k_j).

4) Side Information: Since the companding transform is no longer deterministic, we need to communicate the compander's configuration to the receiver, so that the decompander's parameters can also be adjusted/selected correspondingly. There are J possible configurations which means that $\lceil \log_2 J \rceil$ bits are required for their unique encoding, where $\lceil . \rceil$ represents ceiling function. Hence $\lceil \log_2 J \rceil$ bits of side information will be transmitted with each OFDM symbol. In [11] and [13], enhanced error performance has been reported if the companding operation is eliminated from the receiver, which obviates the need of any side information for these companders.

C. Adaptive Constellation Scaling (ACS)

1) Main Idea: In adaptive constellation scaling (ACS) scheme, the companding transform itself is deterministic. However, *prior to companding, the signal is transformed such that its amplitude distribution matches with that Rayleigh distribution for which the fixed compander is designed.*

2) Design of Constellation Scaling Factor: Let the fixed compander be designed according to $f_A(x) = f_A(x \mid S = \sigma_x^2)$. The samples belonging to an OFDM symbol in j^{th} subset, according to Eq. (18), have amplitude distribution $f_A(x \mid S = \sigma_{xj}^2)$. We need to transform the amplitude of input signal by $h_j(x)$, such that its distribution becomes $f_A(x)$.

The transformation $h_j(x)$ is obtained by using *the distribution modification method* [7], [11]. Let the original amplitude distribution be represented by CDF $F_{A,orig}(x) = 1 - \exp(-x^2/\sigma_{xj}^2)$ and the required distribution be $F_{A,req}(x) = 1 - \exp(-x^2/\sigma_x^2)$. Also, $h_j(x)$ must be monotonically increasing, so that it is uniquely invertible and compatible with the companding transform. Hence, $h_j(x)$ is obtained as follows:

$$h_j(x) = F_{A,req}^{-1}\left(F_{A,orig}(x)\right) = \frac{\sigma_x}{\sigma_{xj}} x \tag{26}$$

The transform $h_j(x)$ is simply scaling of the signal by a constant. This is intuitively satisfying since we are transforming one Rayleigh distribution into another, which means that we are only changing the power of the signal. Moreover, DFT is a linear and unitary operation which means that the scaling can be equivalently done on frequency domain QAM symbols with less complexity. Thus, we are, in effect, *scaling the constellation to change the symbol power*. The scaling factor is selected according to the input symbol power S, as shown in Fig. 8. After comparing the value of S of input symbol with $s_0, s_1, ..., s_J$, the subset index j and hence the transformation $h_j(.)$ is selected for that symbol.

3) Mathematical Definition of the ACS Scheme: The companding transformation with the proposed ACS scheme, using the PLC, is expressed as follows:

$$T_{\mathrm{ACS}}(x) = T_{\mathrm{PLC}}\left(h_j(x); A_c, A_i, k\right), \quad \text{if } x \in \underline{\mathrm{x}}_{\mathbf{n}} \text{ and } S\left(\underline{\mathrm{x}}_{\mathbf{n}}\right) \in \left[s_{j-1}, s_j\right] \tag{27}$$

for $j = 1, 2, ..., J$.

4) Side Information: As in APC, $\lceil \log_2 J \rceil$ bits of side information are transmitted per symbol in ACS as well. The received signal is scaled by $h_j^{-1}(x)$ before demodulation and detection, where j is determined by the side information.

VI. Performance Evaluation

In this section, the proposed APC and ACS schemes are evaluated by applying them to the PLC [6], PEC [5] and ENLC [11]. In order to demonstrate high fidelity of results, the proposed schemes are evaluated for different transforms with various configurations, changing modulation schemes and number of sub-carriers.

A. Simulation Setup and Parameters

OFDM symbols are generated according to the physical layer specifications given in IEEE 802.11a, used in WLAN, and IEEE 802.16d, used in Fixed WiMAX. Parameters are given in Table I. Oversampling factor L is 4. APC and ACS schemes are evaluated for various values of J. Perfect frame synchronization, zero carrier frequency offset and ideal channel estimation are assumed at the receiver. Stanford University Interim-1 (SUI-1) is adopted as the multi-path channel model. In order to assess the proposed schemes in the presence of HPA, solid state power amplifier (SSPA) model is used [2].

B. PAPR Reduction Performance of APC and ACS

Figs. 9, 10 and 11 show CCDF of PAPR curves for APC and ACS schemes. In the figures, 'Orig.' represents conventional companding using the respective transforms.

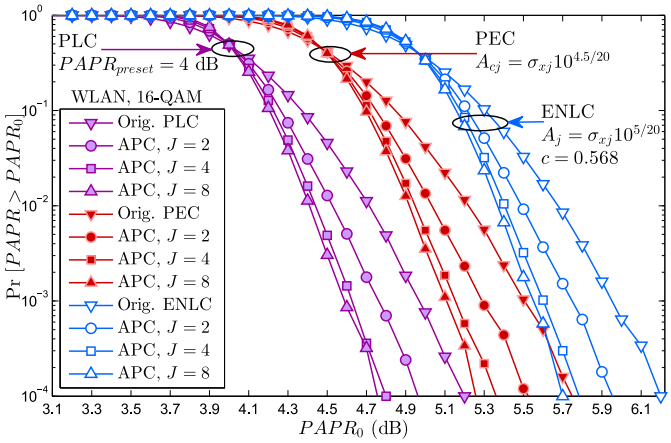

Fig. 9. PAPR reduction performance comparison of conventional companding with APC for WLAN with 16-QAM.

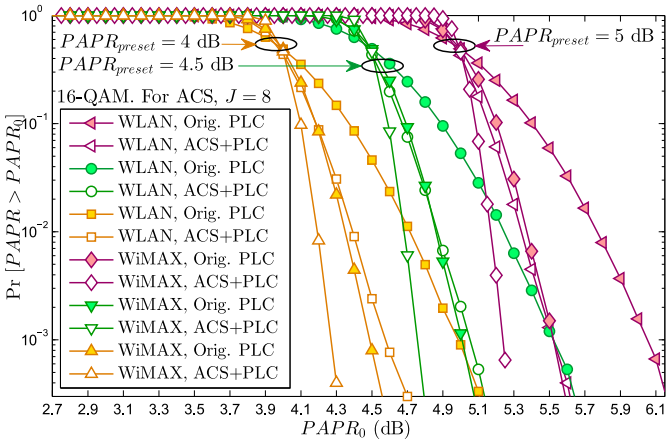

Fig. 10. PAPR reduction performance comparison of conventional companding with ACS scheme for WLAN and WiMAX with 16-QAM.

1) Observations: Fig. 9 shows results for APC schemes with PLC, PEC and ENLC, configured to preset PAPR of 4 dB, 4.5 dB and 5 dB, respectively. It can be seen that as J increases, the PAPR of the output signal comes closer to respective preset values. At CCDF= 10^{-3}, PAPR is reduced by approximately 0.4 dB, 0.42 dB and 0.43 dB for $J = 8$, respectively, as compared to fixed companding.

Fig. 10 shows results for ACS scheme, with $J = 8$, on WLAN and WiMAX with 16-QAM. In case of WLAN, PAPR, at CCDF= 10^{-3}, is reduced by approximately 0.5 dB for each configuration of PLC considered, whereas in case of WiMAX, it is reduced by 0.27 dB. Here, comparative performance of the proposed schemes for different number of sub-carriers can be observed. Since the variance of S in WLAN symbols is larger than that in WiMAX, the amount of PAPR reduction, achieved by effectively reducing this variance, is also greater.

Both the APC and ACS schemes are evaluated for WiMAX with 64-QAM in Fig. 11. For $J = 8$, PAPR at CCDF= 10^{-3} is reduced by approximately 0.35 dB for PEC and 0.41 dB for PLC. It can be seen that in terms of PAPR, APC and ACS perform almost identically.

2) Discussion: Increase in J implies smaller variance of average symbol power in every subset. *Thus the results confirm our assertion that the degradation in conventional companders' performance is due to the variance of average symbol power.* We found that the improvement in PAPR reduction performance is very small in most cases if J is increased beyond 8. Interestingly, with increasing value of J, the CCDF curves approach those obtained for conventional companding on 4-QAM based OFDM. This can be observed by comparing the cases for PLC and ENLC in Figs. 9 and 10 with the simulation results in Fig. 2. This happens because with increasing J, variance of S within each subset is reduced, so the PAPR reduction performance resembles that of 4-QAM, in which S is a constant. Also, it is evident from the results that the schemes can be applied to several configurations of the companders under consideration.

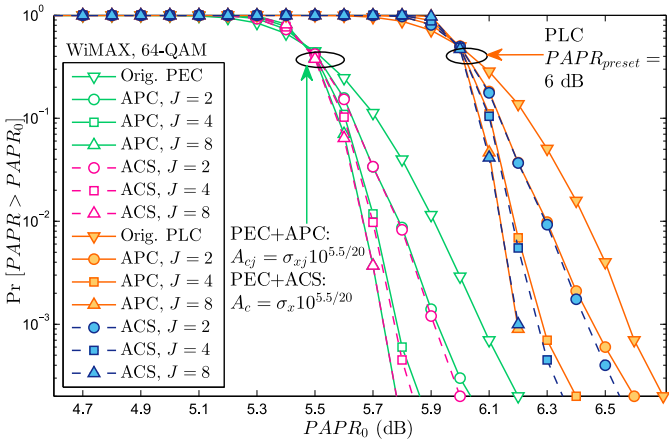

Fig. 11. PAPR reduction performance comparison of conventional companding with APC and ACS for WiMAX with 64-QAM.

3) Comparison of APC and ACS: For same output PAPR, the differences between the two schemes are given below:

- In APC, the average symbol power remains unchanged, i.e., σ_{xj}^2, while its clipped peak power is scaled by a factor σ_{xj}^2/σ_x^2 (by adjusting compander's clipping level).
- In ACS, clipped peak power remains constant. Average symbol power changes from σ_{xj}^2 to σ_x^2.

ACS involves comparatively larger computational overhead due to the additional scaling operation. But it enables all symbols to be transmitted at same average and peak power level, which may facilitate simpler design of the HPA.

C. Error Performance of APC and ACS

Figs. 12-16 show the BER performance for the cases considered in Figs. 9, 10 and 11. AWGN and SUI-1 (Rician) channels are considered for performance evaluation. SSPA model with the parameter $p = 2$ and $p = 4$ is used to evaluate the schemes in the presence of HPA [2]. Smaller value of p indicates higher degree of non-linearity of HPA near the saturation region [2]. The input back-off (IBO) of the HPA is set to be 1 dB higher than the preset PAPR in each case.

1) Observations: As J increases, both the PAPR and BER are reduced. Particularly, the noise floor at high SNR is lowered, which indicates that the noise due to clipping is reduced. This is observed in both the APC and ACS

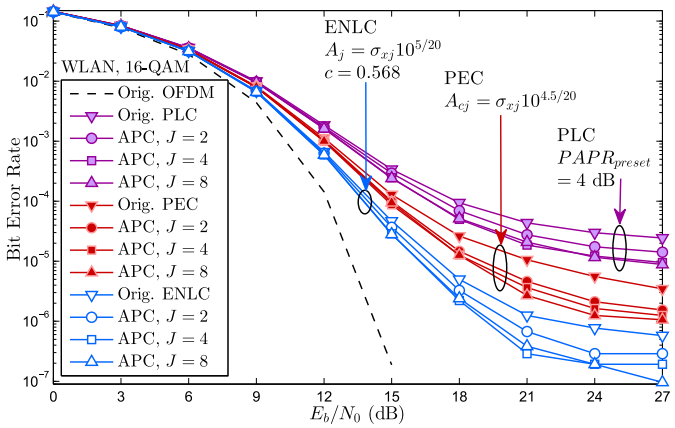

Fig. 12. BER comparison of conventional companding with APC, over AWGN channel, for WLAN with 16-QAM.

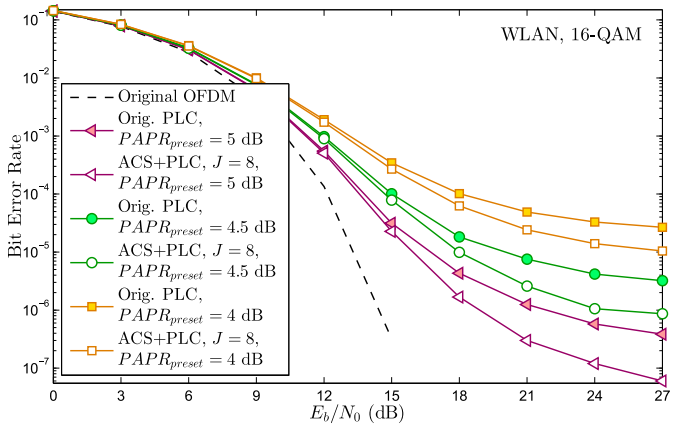

Fig. 13. BER comparison of conventional companding with ACS, over AWGN channel, for WLAN with 16-QAM.

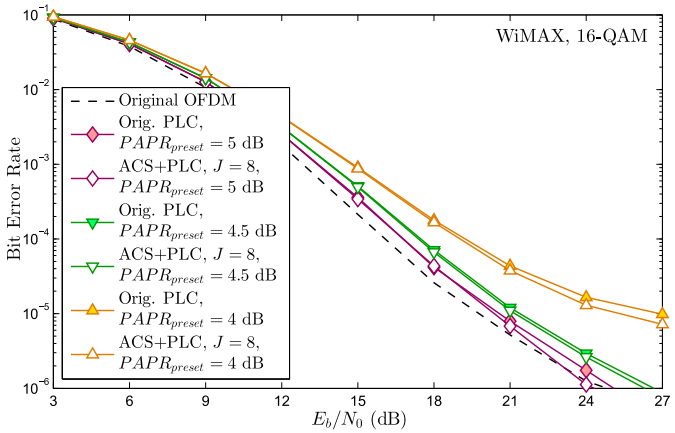

Fig. 14. BER comparison of conventional companding with ACS, over SUI-1 (Rician) channel, for WiMAX with 16-QAM.

schemes. Furthermore, this trend is consistent for AWGN (Figs. 12, 13, 14) and multi-path (Fig. 15) channels. Same trend in BER is also observed in the presence of SSPA (Fig. 16). BER is found to be reduced as compared to conventional companding in all cases considered. *This joint reduction of PAPR and BER is not possible to achieve with conventional, deterministic companding, in which PAPR can only be reduced*

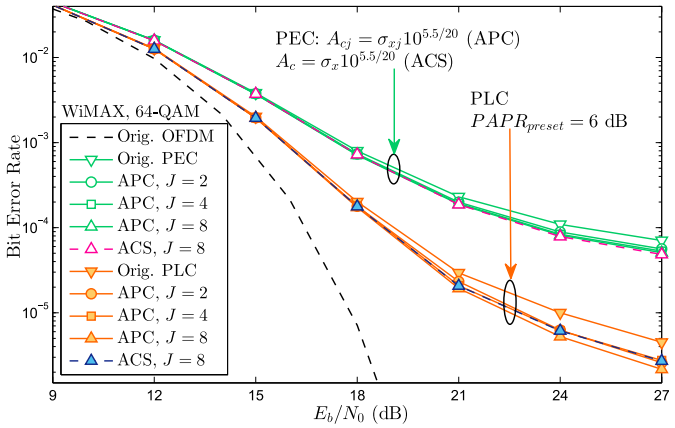

Fig. 15. BER comparison of conventional companding with APC and ACS, over AWGN channel, for WiMAX with 64-QAM.

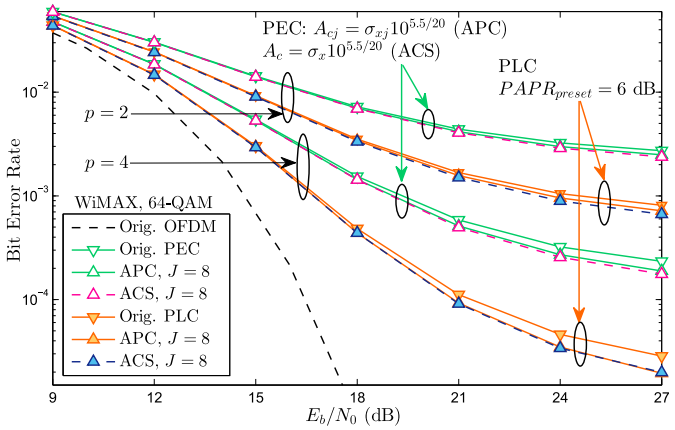

Fig. 16. BER comparison of conventional companding with APC and ACS, with SSPA ($p = 2, 4$, IBO=PAPR+1 dB) over AWGN channel.

at the cost of increased BER. Hence the overall performance of the system is significantly improved.

2) Discussion: In conventional companding, the larger variance of PAPR around the ideal value, as observed in Fig. 2, implies that the compander under-performs for some symbols and over-performs for others. Therefore, in many symbols, conventional companding introduces larger amount of noise than that necessary to achieve the desired PAPR. The proposed schemes enable the compander to adapt to the signal properties. This makes the companding operation more precise. Consequently, the redundant companding/clipping distortion is eradicated to a large extent, which is manifested as the reduction in BER.

D. Out-of-Band Interference (OBI) Levels With APC and ACS

Figs. 17 and 18 show plots of power spectral density (PSD) of companded signals. PSDs are evaluated by averaging several periodogram estimates.

1) Observations: We see that, irrespective of J, the OBI (the increased side-lobe level as compared to original OFDM) due to companding distortion remains same in both the proposed schemes as in corresponding deterministic companding.

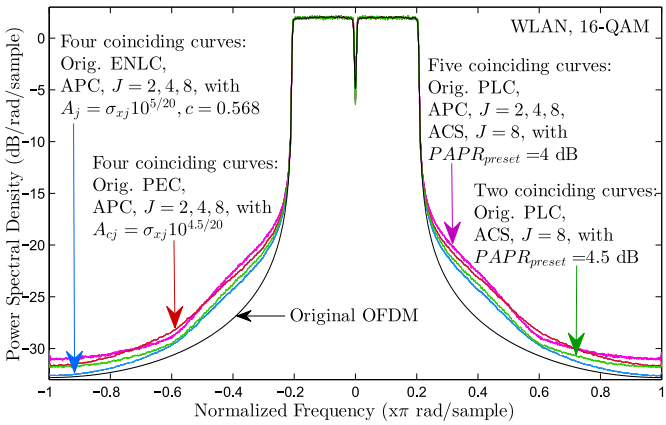

Fig. 17. PSDs of signals transformed by conventional and proposed companding schemes, for WLAN with 16-QAM.

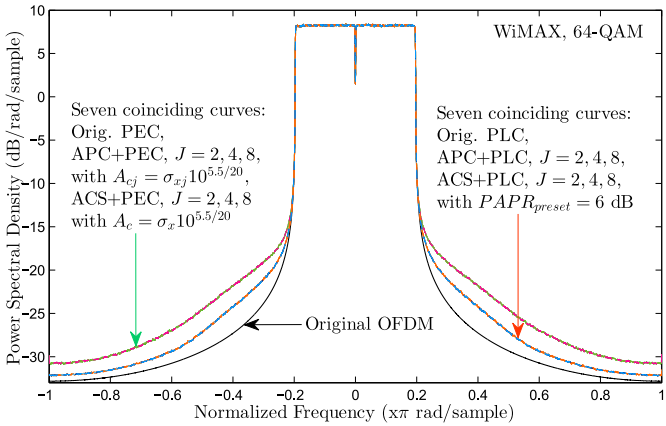

Fig. 18. PSDs of signals transformed by conventional and proposed companding schemes, for WiMAX with 64-QAM.

Also the constant OBI behavior remains consistent with changing transforms, standards and constellations. In conventional companding, PAPR is reduced at the cost of increased OBI, whereas in the proposed schemes, we see that there is no elevation in the average OBI level with decreasing PAPR.

2) Discussion: OBI is related to the average companding noise energy $D = E[(T(x) - x)^2]$. The amount of this noise energy differs from subset to subset, but its overall average remains unaffected. This is explained by the law of total expectation [23], which states that overall average $E[D]$ remains the same irrespective of J, i.e.,

$$E[D] = \sum_{j=1}^{J} E\big[D \mid S \in [s_{j-1}, s_j]\big] \Pr\big[S \in [s_{j-1}, s_j]\big] \qquad (28)$$

We confirmed this property through simulations by evaluating the noise energies for companded OFDM symbols in every subset and comparing their average with the theoretical $E[D]$ in case of PLC.

E. Complexity Analysis of APC and ACS

1) Evaluation of S: This is common in both schemes, as shown in Fig. 8. If symbol-to-energy mapping for the constellation is pre-calculated as a look-up table (LUT), then N_d floating point additions and 1 multiplication are required.

2) Classification of Input Symbol: $J - 1$ comparisons are required to determine the subset index in both the schemes.

3) Parameter Calculation in APC: Compander parameters can be either pre-calculated or adjusted (2 or 3 floating point multiplications), as explained in Section V-B.

4) Scaling in ACS: $4N_d$ floating point multiplications (for scaling complex data symbols at the transmitter and the receiver) are required. Alternatively, *scaled constellations can also be pre-calculated to reduce the complexity*.

Companding is one of the lowest-complexity techniques for PAPR reduction [2], [3] and overhead in APC and ACS is even smaller than the complexity of the transform itself. For example, the relative increase in complexities, as compared to conventional companding, using APC scheme with PEC, ENLC and PLC are 1.5%, 0.3% and 10.4%, respectively (using the complexities given in [5] and [6]). With ACS scheme, complexity is increased by 7.15%, 1.5% and 44.8%, respectively.

F. Bandwidth Efficiency in APC and ACS

As explained in Sections V-B and V-C, $\lceil \log_2 J \rceil$ bits of side information are required in both schemes. Simulation results indicate that significant performance improvement is achieved for $J = 8$, for which only 3 bits are needed. Since the proposed schemes have been implemented on 16 and 64-QAM based OFDM which are already more bandwidth-efficient than 4-QAM, so the relative trade-off is negligibly small. Side information can be either transmitted in the OFDM frame header or it can be modulated on to a reserved sub-carrier.

G. Discussions

1) Duality of APC and ACS: The two proposed schemes are essentially dual of each other. In APC, the compander adapts to the signal's amplitude distribution, whereas in ACS, the signal's amplitude distribution adapts to the compander.

2) Possible Modifications of APC and ACS: In ACS and APC, the symbols in any of the J subsets are transformed independently, so it is also possible to transform them differently or selectively. For example, the ACS scheme can be modified by only applying the scaling on symbols for which $\sigma_{xj}^2 < \sigma_x^2$, so that BER does not increase due to reduced d_{min} in subsets with $\sigma_{xj}^2 > \sigma_x^2$. This will slightly increase the average transmission power and at the same time, computational complexity will be reduced. Therefore, the flexibility in the design methodology can be exploited to meet different performance constraints.

3) Configuration Control in the Proposed Schemes: In conventional companding, PAPR can only be reduced by increasing BER and OBI. In simulation results with APC and ACS, we see that PAPR and BER reduction can also be controlled by specifying J. This implies that the APC and ACS schemes offer the additional flexibility to trade computational complexity and channel throughput (amount of side information) for performance gain. Consequently, they are more tractable for obtaining various operating conditions for the system, which enhances the system's adaptability to changing input and channel conditions and application requirements.

4) Advantages of the Proposed Classification Method: The overhead on channel throughput is small (see Section VI-F) due to the classification method used in the proposed schemes. If the compander were designed to adjust differently for every single value of S, instead of using only J adaptations, the required number of bits for WLAN with 16-QAM and 64-QAM would be 7 and 10, respectively. For WiMAX, required number of bits would be 9 and 12 for 16 and 64-QAM, respectively. Furthermore, the low-complexity implementations suggested in Section VI-E would also not be feasible. It should be noted that errors in side information also lead to increase in BER. Thus, smaller amount of side information not only reduces the throughput loss, but the probability of occurrence of such errors is also diminished.

VII. Conclusion

In this paper, two novel schemes are presented to enhance the PAPR reduction performance of companding transforms in OFDM systems employing higher order QAM. Probabilistic model of the average OFDM symbol power and amplitude is developed and utilized in the design of the proposed schemes. Performance gain is achieved by making the companding operation adapt to changing amplitude distribution, which involves adjusting it according to the average power of input OFDM symbols during application run-time. Simulation results show that the proposed schemes have the unique capability of jointly reducing the PAPR and BER, while keeping OBI unchanged. Hence, the overall performance of the system is significantly enhanced. The schemes have been effectively applied to several state-of-the-art companders. Furthermore, the schemes also enhance the system's adaptability by providing more possible operating conditions than those viable with conventional companding.

References

[1] T. Hwang, C. Yang, G. Wu, S. Li, and G. Y. Li, "OFDM and its wireless applications: A survey," *IEEE Trans. Veh. Technol.*, vol. 58, no. 4, pp. 1673–1694, May 2009.

[2] Y. Rahmatallah and S. Mohan, "Peak-to-average power ratio reduction in OFDM systems: A survey and taxonomy," *IEEE Commun. Surveys Tuts.*, vol. 15, no. 4, pp. 1567–1592, Dec. 2013.

[3] T. Jiang and Y. Wu, "An overview: Peak-to-average power ratio reduction techniques for OFDM signals," *IEEE Trans. Broadcast.*, vol. 54, no. 2, pp. 257–268, Jun. 2008.

[4] Y. Wang, C. Yang, and B. Ai, "Iterative companding transform and filtering for reducing PAPR of OFDM signal," *IEEE Consum. Electron. Mag.*, vol. 61, no. 2, pp. 144–150, May 2015.

[5] M. Hu, Y. Li, Y. Liu, and H. Zhang, "Parameter-adjustable piecewise exponential companding scheme for peak-to-average power ratio reduction in orthogonal frequency division multiplexing systems," *IET Commun.*, vol. 8, no. 4, pp. 530–536, Mar. 2014.

[6] M. Hu, Y. Li, W. Wang, and H. Zhang, "A piecewise linear companding transform for PAPR reduction of OFDM signals with companding distortion mitigation," *IEEE Trans. Broadcast.*, vol. 60, no. 3, pp. 532–539, Sep. 2014.

[7] S. P. DelMarco, "General closed-form family of companders for PAPR reduction in OFDM signals using amplitude distribution modification," *IEEE Trans. Broadcast.*, vol. 60, no. 1, pp. 102–109, Mar. 2014.

[8] S. Peng, Y. Shen, and Z. Yuan, "PAPR reduction of multi-carrier systems with simple nonlinear companding transform," *Electron. Lett.*, vol. 50, no. 6, pp. 473–475, Mar. 2014.

[9] Y. Wang, J. Ge, L. Wang, J. Li, and B. Ai, "Nonlinear companding transform for reduction of peak-to-average power ratio in OFDM systems," *IEEE Trans. Broadcast.*, vol. 59, no. 2, pp. 369–375, Jun. 2013.

[10] Y. Wang, L.-H. Wang, J.-H. Ge, and B. Ai, "Nonlinear companding transform technique for reducing PAPR of ODFM signals," *IEEE Trans. Consum. Electron.*, vol. 58, no. 3, pp. 752–757, Aug. 2012.

[11] Y. Wang, L.-H. Wang, J.-H. Ge, and B. Ai, "An efficient nonlinear companding transform for reducing PAPR of OFDM signals," *IEEE Trans. Broadcast.*, vol. 58, no. 4, pp. 677–684, Dec. 2012.

[12] S.-S. Jeng and J.-M. Chen, "Efficient PAPR reduction in OFDM systems based on a companding technique with trapezium distribution," *IEEE Trans. Broadcast.*, vol. 57, no. 2, pp. 291–298, Jun. 2011.

[13] J. Hou, J. Ge, D. Zhai, and J. Li, "Peak-to-average power ratio reduction of OFDM signals with nonlinear companding scheme," *IEEE Trans. Broadcast.*, vol. 56, no. 2, pp. 258–262, Jun. 2010.

[14] J. Hou, J. H. Ge, and J. Li, "Trapezoidal companding scheme for peak-to-average power ratio reduction of OFDM signals," *Electron. Lett.*, vol. 45, no. 25, pp. 1349–1351, Dec. 2009.

[15] S. A. Aburakhia, E. F. Badran, and D. A. E. Mohamed, "Linear companding transform for the reduction of peak-to-average power ratio of OFDM signals," *IEEE Trans. Broadcast.*, vol. 55, no. 1, pp. 155–160, Mar. 2009.

[16] T. Jiang, W. Yao, P. Guo, Y. Song, and D. Qu, "Two novel nonlinear companding schemes with iterative receiver to reduce PAPR in multi-carrier modulation systems," *IEEE Trans. Broadcast.*, vol. 52, no. 2, pp. 268–273, Jun. 2006.

[17] T. Jiang, Y. Yang, and Y.-H. Song, "Exponential companding technique for PAPR reduction in OFDM systems," *IEEE Trans. Broadcast.*, vol. 51, no. 2, pp. 244–248, Jun. 2005.

[18] T. Jiang and G. Zhu, "Nonlinear companding transform for reducing peak-to-average power ratio of OFDM signals," *IEEE Trans. Broadcast.*, vol. 50, no. 3, pp. 342–346, Sep. 2004.

[19] A. Doufexi *et al.*, "A comparison of the HIPERLAN/2 and IEEE 802.11a wireless LAN standards," *IEEE Commun. Mag.*, vol. 40, no. 5, pp. 172–180, May 2002.

[20] J. G. Andrews, A. Ghosh, and R. Muhamed, *Fundamentals of WiMAX: Understanding Broadband Wireless Networking*. Upper Saddle River, NJ, USA: Prentice Hall, 2007.

[21] J. Zyren and W. McCoy, *Overview of the 3GPP Long Term Evolution Physical Layer*, Freescale Semicond. Inc., Austin, TX, USA, White Paper, 2007.

[22] *Digital Video Broadcasting: Framing Structure, Channel Coding, and Modulation for Digital Terrestrial Television*, ETSI EN 300 744 v1.4.1, 2001.

[23] A. León-García, *Probability and Random Processes for Electrical Engineering*. Reading, MA, USA: Addison-Wesley, 1994.

Sana Mazahir received the B.E. degree in electrical engineering and the master's degree in electrical engineering (DSP and communications) from the College of Electrical and Mechanical Engineering, National University of Sciences and Technology (NUST), Rawalpindi, Pakistan, in 2013 and 2015, respectively. She is currently a Research Assistant with the System Analysis and Verification Laboratory, NUST. Her research interests include signal construction and processing for wireless communications and stochastic modeling and analysis of systems and approximate computing.

Shahzad Amin Sheikh received the B.S. degree in electrical engineering from Eastern Mediterranean University, North Cyprus, in 1995, the master's degree in electrical engineering from the University of New South Wales, Sydney, Australia, in 2002, and the Ph.D. degree in information and communication systems engineering from Southwest Jiaotong University, Chengdu, China, in 2008. He is currently a Faculty Member with the Electrical Engineering Department, College of Electrical and Mechanical Engineering, National University of Sciences and Technology, Rawalpindi, Pakistan. His research interests are blind channel equalization and estimation and DSP and its applications in digital communications and biomedical engineering.